# Supplemental Material

## Electrostatic shaping of magnetic transition regions in $La_{0.7}Sr_{0.3}MnO_3$

Qianqian Lan[1,2], Chuanshou Wang[3], Lei Jin[1], Michael Schnedler[1], Lars Freter[1], Kurt Fischer[4] Jan Caron[1], Xian-Kui Wei[1], Thibaud Denneulin[1], András Kovács[1], Philipp Ebert[1], Xiaoyan Zhong[5,6,7], Rafal E. Dunin-Borkowski[1]

[1] Ernst Ruska-Centre for Microscopy and Spectroscopy with Electrons (ER-C 1) and Peter Grünberg Institut (PGI-5), Forschungszentrum Jülich GmbH, 52425 Jülich, Germany

[2] National Center for Electron Microscopy in Beijing, Key Laboratory of Advanced Materials (MOE), School of Materials Science and Engineering, Tsinghua University, Beijing 100084, People's Republic of China

[3] Department of Physics, Southern University of Science and Technology, Shenzhen 518055, People's Republic of China

[4] Department of Mechanical and Electrical Engineering, National Institute of Technology, Tokuyama College, Gakuendai, Shunan, Yamaguchi, 745-8585, Japan

[5] TRACE EM Unit and Department of Materials Science and Engineering, City University of Hong Kong, Kowloon 999077, Hong Kong SAR, People's Republic of China.

[6] City University of Hong Kong Shenzhen Futian Research Institute, Shenzhen 518048, People's Republic of China.

[7] Nanomanufacturing Laboratory, City University of Hong Kong, Shenzhen Research Institute, Shenzhen 518057, People's Republic of China

**Film deposition.** A 200 nm thick $La_{0.7}Sr_{0.3}MnO_3$ (LSMO) thin film was grown on a 0.5 wt% Nb-doped $SrTiO_3$ (STO) (001) substrate using pulsed laser deposition. The nominally $La_{0.7}Sr_{0.3}MnO_3$ target was ablated using a KrF excimer laser (wavelength 248 nm) with an energy density of 1 J/cm$^2$ and a repetition rate of 5 Hz while the substrate temperature and oxygen pressure were maintained at 720 $^o$C and 100 mTorr, respectively. Within the growth of the LSMO film a growth interruption occurred, which is at the origin of the Mn composition change.

**Macroscopic magnetism measurement.** Figure S1 shows a *macroscopic* measurement of the magnetization of the 200-nm-thick LSMO layer recorded using a superconducting quantum interference device (SQUID) magnetometer between 90 and 300 K with a 500 Oe magnetic field applied parallel to the LSMO/STO interface. The temperature at which the magnetization-temperature (*M*-*T*) curve (black line) reaches zero, i.e. 339 K, corresponds to the critical temperature ($T_C$) for the ferromagnetic (FM) to paramagnetic (PM) transition and

is typical for LSMO films [1-3]. The derivative of the magnetization curve d*M*/d*T* (blue line) reveals, however, besides the minimum at 339 K and a second local minimum at 279 K, suggesting the presence of an additional magnetic phase transition with a different $T_C$.

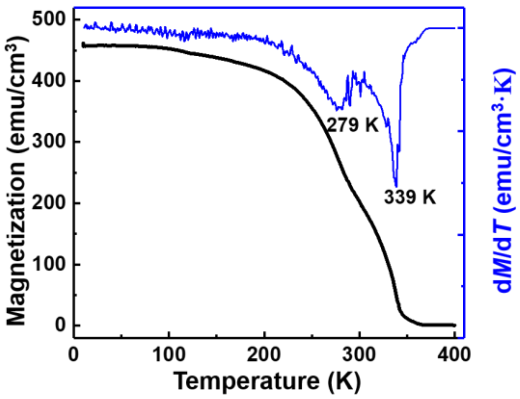


***Figure S1:*** *Macroscopic magnetization measurement of the 200-nm-thick LSMO film on STO performed using SQUID magnetometry in a magnetic field of 500 Oe applied parallel to the LSMO/STO interface, showing a magnetization-temperature (M-T) curve (black) and its derivative (dM/dT) (blue). The measurement shows a primary transition at 339 K and an additional transition at approximately 279 K.*

**Specimen preparation for TEM.** Cross-sectional TEM specimens were prepared using FIB milling in a FEI Helios Nanolab 400s dual-beam system. Ga ion beam surface damage was reduced by using 500 eV Ar ion beam sputtering in a Fischione Nanomill 1040 system. The thickness of the lamella in the electron beam direction was measured to be ~120 nm measured in FIB system.

**Microstructure and electronic structure characterization.** High-angle annular dark-field (HAADF) scanning TEM (STEM). imaging and energy-dispersive X-ray (EDX)/ electron energy-loss spectroscopy (EELS) mapping were carried out at 200 kV in an FEI Titan G2 80-200 microscope equipped with in-column (Super-X) EDX detectors, a high brightness field emission gun (XFEG), a spherical aberration ($C_S$) corrector for the probe forming system and a Gatan Enfinium ER (model 977) electron energy-loss spectrometer with DUAL EELS.

**Off-axis electron holography (EH).** Off-axis EH was performed in an image-$C_S$-corrected FEI Titan 80-300 microscope equipped with two electron biprisms at 300 kV. A liquid-nitrogen-cooled double tilt specimen holder (Gatan model 636) was used to vary the specimen temperature between 93 and 370 K. Off-axis electron holograms were recorded in magnetic-field-free conditions using a direct electron-counting camera (Gatan K2 IS). The phase shift of an electron wave reconstructed from hologram resulting from the presence of magnetic and electric fields. In order to separate the two contributions to the phase shift, the specimen was tilted to ±70 º and the magnetic field of the conventional objective lens of the microscope was used to magnetize it in opposite directions in a field of about 1.5 T. Half of the sum and

half of the difference between aligned phase images reconstructed from such pairs of off-axis electron holograms were used to determine the electrostatic and magnetic contributions to the phase, respectively [4,5] (see Fig. S2). The electrostatic contribution to the phase is based on the mean inner and electrostatic potentials of the specimen integrated in the electron beam direction, while the gradient of the magnetic contribution to the phase is proportional to the strength and direction of the in-plane magnetic induction projected in the electron beam direction. The projected width of the film-substrate interface was approximately 1.7 nm (due to a tilt of approximately 1° perpendicular to the interface to minimize diffraction contrast).

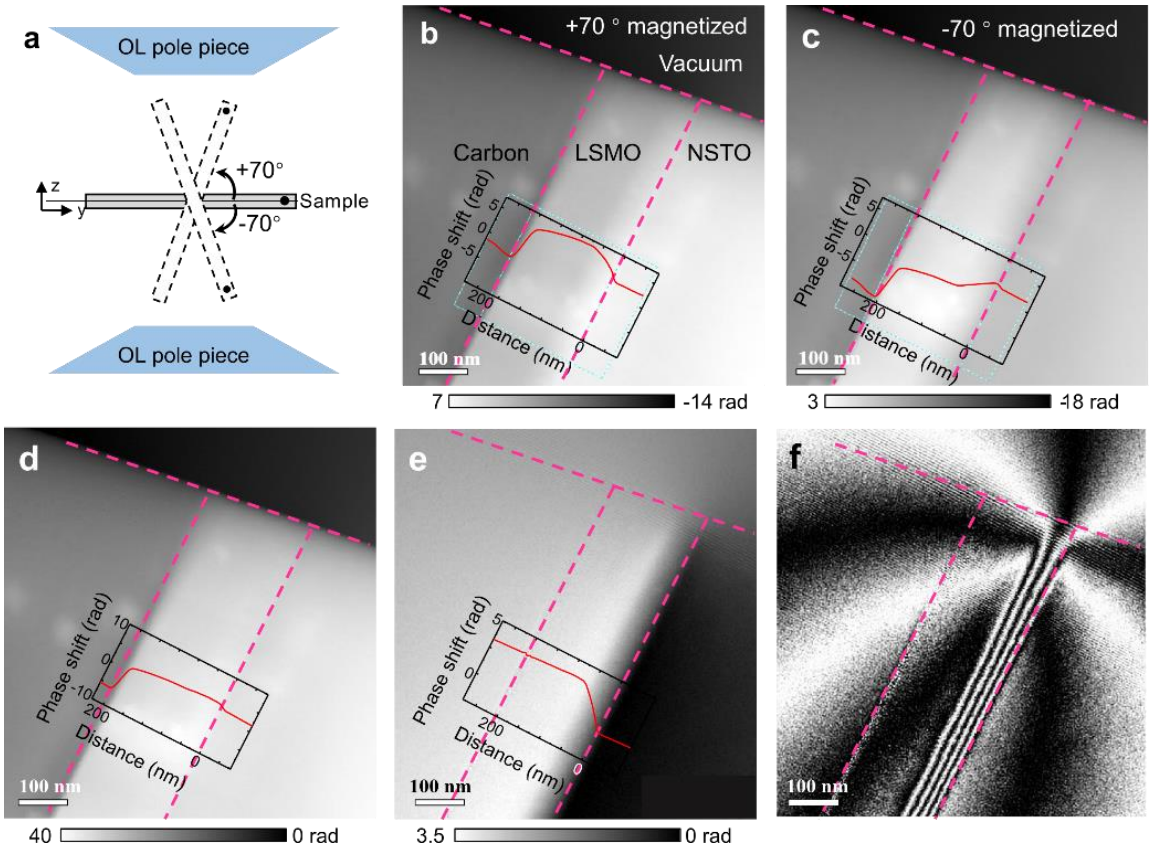


***Figure S2.*** *(a) Schematic diagram illustrating the tilt of the specimen during magnetizing using the magnetic field* ***H*** *in z direction between the pole pieces (objective lens). After magnetizing, the tilt and the magnetic field are reduced to zero before electron holograms of the remanence magnetization state within specimen are acquired. The magnetizing is done for positive and negative 70° tilt, yielding a parallel and antiparallel magnetization of the specimen, respectively. (b, c) Pair of reconstructed electron phase images of the* $La_{0.7}Sr_{0.3}MnO_3$ *(LSMO) film acquired for the specimen magnetized parallel and antiparallel. The insets illustrate the line profiles of the respective electron phase shift. (d) Mean inner and electrostatic potential and (e) magnetic contributions to the phase with the respective line profiles of the electron phase as insets. (f) Magnetic induction map generated from (e) with a contour spacing of* $\pi$ *radians. Slight misalignment artifacts from removing the mean inner potential contribution to the phase are visible at the specimen edge in some images.*

**Electron holographic tomography.** For the determination of the out-of-plane magnetization component we rotated the TEM lamella with respect to the electron beam direction as shown schematically in Fig.S3a. With this in mind the phase change induced by the magnetization in the lamella is given by [6]

$$\frac{\mathrm{d}\varphi}{dx} \sim M_{\mathrm{in}} \cdot d_{\mathrm{eff}} = M \cdot d \cdot cos(\beta) \cdot \big(1 - tan(\beta)tan(\alpha)\big) \qquad (1)$$

with α being the tilt angle (in the tomographic rotation) of the lamella and β being the rotation of the magnetization off the in-plane direction. For only in-plane magnetization (β=0), $\frac{\mathrm{d}\varphi}{dx}$ is constant and independent of the tilt angle α of the lamella.

The experimental results of the electron holographic tomography are shown in Fig. S3b as a function of the tilt angle α for sublayers A and B at 94 K and for sublayer A at 295 K (sublayer B is at 295 K paramagnetic already). It is obvious that the values of $\frac{\mathrm{d}\varphi}{dx}$ are constant for every measurement. The dashed lines show fits of the above relation of $\frac{\mathrm{d}\varphi}{dx}$ vs. α and reveal values for the out-of-plane rotation β of the magnetization of 2.7°±1.2° (sublayer A at 295 K), 0.95°±1.1° (sublayer A at 94 K), and 0.1°±1.1° (sublayer B at 94 K) only. Under consideration of the error bars and the absolute values no relevant out-of-plane component of the magnetization exists. Hence, the orientation of magnetization of the two sublayers is in-plane and parallel.

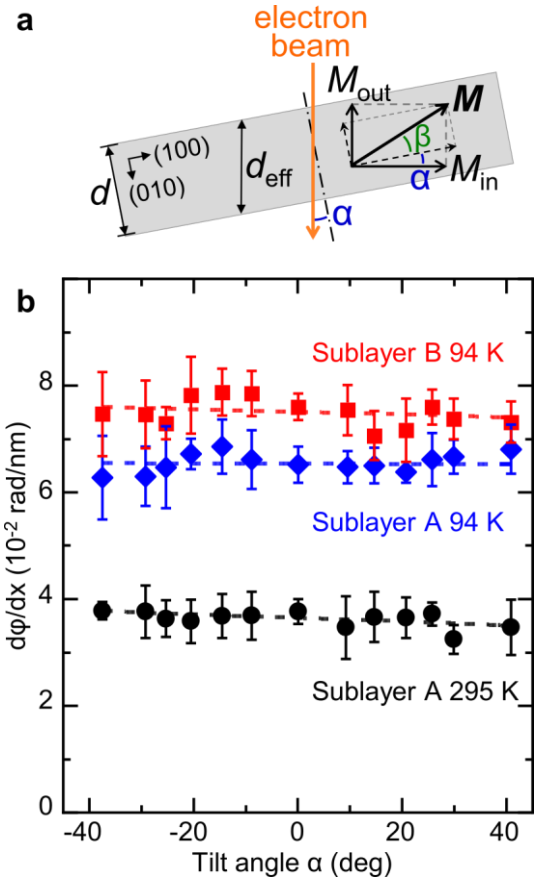


***Fig. S3**: (a) Schematic of the effect of tilt on the magnetization projected on the plane perpendicular to the electron beam direction. This results in Eq. (1) describing the tilt dependence of the gradient of the electron phase shift. (b) Electron holographic tomography:*

*Gradient of the electron phase vs tilt angle α (tilt axis parallel to [001] direction) for sublayers A and B at different temperatures. The data reveals that the magnetization has no out-of-plane component.*

**Absense of structural changes.** Figure S4a shows a selected area electron diffraction (SAED) pattern recorded from the complete LSMO film. Neither splitting nor elongation of the (100) and (001) diffraction spots is evident, *i.e.*, there is no measurable difference in lattice constant between the two sublayers. This is consistent with the lattice constants measured by fitting Gaussians to atomic contrast in high-angle annular dark-field (HAADF) scanning TEM (STEM) images and averaging the measurements parallel to the interface (Fig. S4b): The lattice constant *a* (parallel to the LSMO/STO interface) remains unchanged at 3.931±0.048 Å throughout the STO substrate and LSMO layers. The perpendicular lattice constant *c* is 3.817±0.066 Å and 3.820±0.055 Å in sublayers A and B, respectively, indicating that there is no measurable change in structure and biaxial strain between the LSMO sublayers, eliminating in our case lattice or phase changes as an origin of the magnetization change.

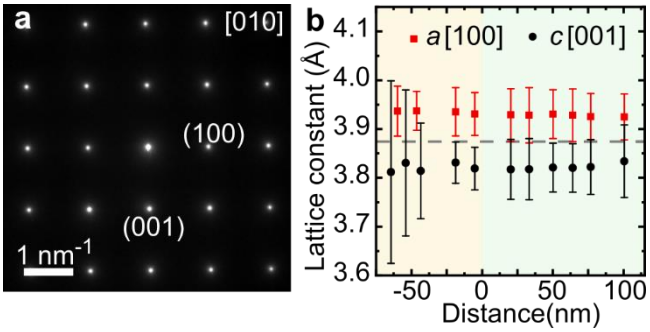


***Fig. S4****: Microstructural analysis. (a) SAED pattern of the LSMO layer (including both sublayers). (b) Lattice constants a (red) and c (black) vs. distance in growth direction obtained from HAADF-STEM images, indicating no detectable change of the lattice constant or symmetry.*

## References


[1] M. Huijben, L. W. Martin, Y. H. Chu, M. B. Holcomb, P. Yu, G. Rijnders, D. H. A. Blank, and R. Ramesh, Phys. Rev. B **78**, 094413 (2008).

[2] K. J. O'Shea, D. A. MacLaren, D. McGrouther, D. Schwarzbach, M. Jungbauer, S. Huhn, V. Moshnyaga, and R. L. Stamps, Nano Lett. **15**, 5868 (2015).

[3] S. Chen, C. Guan, S. Ke, X. Zeng, C. Huang, S. Hu, F. Yen, H. Huang, Y. Lu, and L. Chen, ACS Appl. Mater. Interfaces **10**, 18029 (2018).

[4] R. E. Dunin-Borkowski, M. R. McCartney, D. J. Smith, and S. S. P. Parkin, Ultramicroscopy **74**, 61 (1998).

[5] T. Kasama, M. S. Moreno, R. E. Dunin-Borkowski, S. B. Newcomb, N. Haberkorn, J. Guimpel, and P. A. Midgley, Appl. Surf. Sci. **252**, 3977 (2006).

[6] T. Kasama, M. Beleggia, and R. E. Dunin-Borkowski, *Electron holography of magnetic materials* (intechopen London, United Kingdom, 2011), p. 57-61.